European Journal of Medicinal Chemistry 63 (2013) 321–332

Contents lists available at SciVerse ScienceDirect

European Journal of Medicinal Chemistry

journal homepage: http://www.elsevier.com/locate/ejmech

Original article

Molecular determinants for nuclear receptors selectivity: Chemometric analysis, dockings and site-directed mutagenesis of dual peroxisome proliferator-activated receptors α/γ agonists

Antonio Carrieri [a,*], Marco Giudici [b], Mariagiovanna Parente [a], Mario De Rosas [c], Luca Piemontese [a], Giuseppe Fracchiolla [a], Antonio Laghezza [a], Paolo Tortorella [a], Giuseppe Carbonara [a], Antonio Lavecchia [d], Federica Gilardi [b], Maurizio Crestani [b], Fulvio Loiodice [a]

[a] Dipartimento di Farmacia-Scienze del Farmaco, Università degli studi di Bari 'Aldo Moro', via E. Orabona 4, 70125 Bari, Italy
[b] Dipartimento di Scienze Farmacologiche e Biomolecolari, Università degli Studi di Milano, via Balzaretti 9, 20133 Milano, Italy
[c] Dipartimento di Scienze Biomediche, Università di Foggia, viale L. Pinto 7, 71100 Foggia, Italy
[d] Dipartimento di Chimica Farmaceutica e Tossicologica, 'Drug Discovery' Laboratory, Università degli Studi di Napoli 'Federico II', Via D. Montesano, 49, 80131 Napoli, Italy

ARTICLE INFO

Article history:
Received 30 October 2012
Received in revised form
28 January 2013
Accepted 14 February 2013
Available online 24 February 2013

Keywords:
Peroxisome proliferator-activated receptors
Selectivity
Docking
GRIND
3D-QSAR
Mutagenesis

ABSTRACT

A series of previously synthesized chiral derivatives of clofibric and phenylacetic acids, acting as dual agonists towards the peroxisome proliferator-activated receptors (PPARs) α and γ, was taken into account, and the efficacy of these compounds was analyzed by means of 2D-, 3D-QSAR and docking studies with the goal to gain deeper insights into the three-dimensional determinants governing ligands selectivity for PPARs. By multiregressional analysis a correlation between the lipophilicity and PPARα activity was found, whereas for PPARγ the correlation was achieved once efficacy was related to the presence of polar groups on agonists scaffold. Docking of these compounds further corroborated this hypothesis, and then provided a valid support for subsequent chemometric analysis and pharmacophore models development for both receptors subtypes. Computational results suggested site directed mutagenesis experiments which confirmed the importance of amino acid residues in PPAR activity, allowing the identification of critical hotspots most likely taking over PPARs selectivity.

1. Introduction

Cardiovascular disease (CVD) still remains worldwide the leading cause of death, with more than 17 million people died, mainly due to heart attacks or strokes, according to the latest World Health Organization reports [1]. CVDs are related to different factors such as atherosclerosis or cardiac deficiency, but also to other risks like behavioural habits (i.e. tobacco, inactivity, alcohol, unhealthy diet) or other sources (diabetes, abdominal obesity, high blood pressure, sugar and lipid) [2,3]. These latest incidences are directly related to the so called metabolic syndrome (MS), a complex of interrelated risk factors, often observed in the westernized countries, including also atherogenic dyslipidemia, insulin resistance and glucose intolerance, proinflammatory and prothrombotic state [4,5]. It is widely accepted that changing styles of life and habits might largely decrease the incidence of MS, but proper therapeutic interventions are still an urgent need [6–8].

Several drugs, with diverse chemical clichés and different mechanism of action, have already been marketed and currently used for the treatment of CVDs [3,9,10]. Most recently the exploit of compounds acting as binders of the Peroxisome Proliferator-Activated Receptors (PPARs) resulted a very promising approach [9–11]. PPARs are ligand-activated transcription factors belonging to the nuclear hormone receptor superfamily which activate transcription of target genes as heterodimers with the partner retinoid X receptor (RXR). Subtypes that are the products of

Abbreviations: MS, metabolic syndrome; CVD, cardiovascular disease; LBD, ligand-binding domain; SDM, site directed mutagenesis; DOPE, discrete optimized protein energy; MIFs, molecular interaction fields; GRIND, GRID independent descriptors; DRY, hydrophobic probe; HBA, hydrogen bond acceptor; HBD, hydrogen bond donor; SHP, shape probe; LOO, leave-one-out; DPP, diphenyl pocket; BPP, benzophenone pocket.

* Corresponding author. Tel.: +39 080 5442638; fax: +39 080 5442724.
E-mail addresses: antonio.carrieri@uniba.it, carrieri@farmchim.uniba.it (A. Carrieri).

0223-5234/$ – see front matter © 2013 Elsevier Masson SAS. All rights reserved.
http://dx.doi.org/10.1016/j.ejmech.2013.02.015

distinct genes are commonly designated PPARα, PPARγ, and PPARδ. The human PPAR genes characterized to date reveal a common organization of the translated region in six coding exons (A–F), with the latest two exons encoding for a ligand-binding domain (LBD) [12,13]. This area has also been fully characterized by crystallographic studies highlighting the main structural features of the PPAR surface.

The presence of three isoforms lies beneath the evidence of different physiological functions elicited by the three receptors, involved therefore in a pool of pathological instances. Nowadays, dual-acting PPARα/γ agonists are considered a very attractive option in the treatment of dyslipidemic type 2 diabetes [11].

However, even though a relatively high number of dual agonists have been described so far, a balanced PPARα/γ activator is still a missed weapon in the arsenal of CVDs research [14,15].

In this stimulating scenario, we recently synthesized a series of chiral clofibric and phenylacetic acid analogues capable to selectively activate both PPARα and PPARγ [16–21]. Furthermore, the X-ray crystal of the PPARγ-LBD in complex with the most promising derivative was also solved [22], highlighting a novel binding cleft on the LBD, distinctive for the (*S*)-enantiomer, crucial for the heterodimer complex formation, recruiting transcription coactivators, and regulating the transcription of genes involved in the control of lipid and carbohydrate metabolism [23,24].

To get fresh insights into PPAR activation elicited by our dual agonists, and to deem the molecular determinants most likely governing receptor selectivity, here we present ligand and structure-based computational studies carried out with a combination of complementary approaches, successfully applied in the past by some of us [25–27], based on QSAR, docking studies and chemometric analysis. Our aim was to explore uncharted region of the chemical space, to depict plausible pharmacophore models for our targets, and to transfer the information achieved from the modelling, to site directed mutagenesis (SDM) assays capable to supply experimental proofs regarding the proposed hypothesis.

2. Methods

2.1. Molecular modelling

Standard bond lengths and valence angles for the molecular scaffold of the (*S*)-enantiomers of the selected compounds (Table 1) were achieved upon a conjugate gradient minimization of the ionized structures, mimicking water with the solvent continuum method, according to the OPLS2005 force field parameters implemented in the MacroModel software package [28].

2D-QSAR statistical analysis was performed relating pA with the fifty molecular descriptors implemented in the QikProp software tool [29] providing a complete level of information with different 1D and 2D indices related not only to physicochemical, but also to topological, geometrical, quantum chemical and pharmacokinetics features of the ligand by multiple linear regression. Each single QikProp descriptor was linearly related to pAs, and a filtering was carried out selecting, according to a $r^2 \geq 0.6$, the most significant regressions (Tables 2 and 3).

The two targets were prepared as follows: PPARα/BMS-631707 and PPARγ/**1b** complexes were retrieved from the Protein Data Bank (PDB codes: 2REW and 3B3K respectively) [22,30]. Apo forms were generated by removing non-protein portion, polar hydrogens were added and their relative position optimized through the protein preparation wizard implemented in the Maestro software package [31]. Electrostatic charges were calculated according to the AMBER UNITED force field by means of the AutoDockTools [32]. The two missing loops (Lys232-Asn236 and Ile236-Val255) in the 2REW structure were reconstructed using the loop building routine in Modeller 9.7 software package [33]. The *refine_loop* method was employed to generate their atomic coordinates. In the *refine_loop* method, 500 initially randomized models were created and the best model was selected on the basis of DOPE (Discrete Optimized Protein Energy) assessment score.

The binding site mapping was done on both PPARα and PPARγ receptors calculating the molecular interaction fields (MIFs) by means of GRID 22c [34]. The MIFs identify in the protein binding

Table 1
Structure and activity of **CLOF** (a), **PHEN** (b) and **NAPH** (c) derivatives.

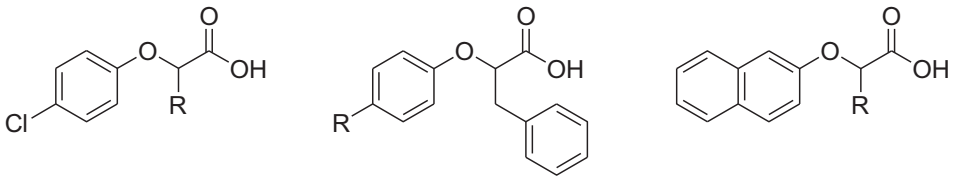

Cmp	R	$pA_{PPAR\alpha}$[a]	$pA_{PPAR\gamma}$[a]	Cmp	R	$pA_{PPAR\alpha}$[a]	$pA_{PPAR\gamma}$[a]
1a	$Ph(CH_2)_2$	5.62	5.15	**3b**	$Ph(CH_2)_2$	6.82	6.40
2a	$Ph(CH_2)_3$	6.23	6.04	**4b**	PhO	6.05	5.80
3a	4-Cl–$Ph(CH_2)_3$	6.20	6.50	**5b**	CH_2OH	4.54	4.59
4a	$PhOCH_2$	5.60	5.78	**6b**	CH_3CH_2	6.15	5.44
5a	$PhO(CH_2)_2$	5.52	5.90	**7b**	CH_3CO	4.87	4.91
6a	4-PhO–$PhCH_2$	6.06	7.57	**8b**	CH_3O	5.60	4.70
7a	4-Ph–$PhCH_2$	5.95	7.31	**9b**	CF_3	6.30	6.05
8a	4-(2-thienyl)-$PhCH_2$	6.23	7.19	**10b**	Cl	[b]	[b]
9a	4-CF_3–$PhCH_2$	5.44	6.38	**11b**	4-Cl–Ph	5.41	5.05
10a	$PhCH_2$	5.41	5.57	**1c**	$PhCH_2$	5.85	5.82
1b	Ph	6.72	6.25	**2c**	$CH_3(CH_2)_2$	5.08	5.14
2b	$PhCH_2$	7.96	6.24				

[a] Measured as $-\log EC_{50}$ (μM) in cell-based transactivation assay of GAL4-PPAR chimeric receptors expressed in transiently transfected HepG2 cells according to a previously reported procedure (J.M. Lehmann, L.B. Moore, T.A. Smith-Oliver, W.O. Wilkison, T.M. Willson, S.A. Kliewer, J. Biol. Chem. 270 (1995) 12953–12956).
[b] Compound **10** might be equally referred to **a** or **b**.

Table 2
$pA_{PPAR\alpha}$ r^2 values of the QikProp descriptors for **CLOF** and **PHEN** classes.

$pA_{PPAR\alpha}$	***accptHB***	***ACxDN5SA***	***CIQPlogS***	***CNS***	***dip2V***	***Dipole***
CLOF	0.078	0.203	0.265	0.000	0.026	0.006
PHEN	0.517	0.510	**0.724**	0.469	0.227	0.177
	donorHB	***EAeV***	***FISA***	***FOSA***	***Glob***	***HumOrAbs***
CLOF	0.000	0.008	0.179	0.162	0.281	0.167
PHEN	0.267	0.009	0.420	0.011	0.578	0.077
	in56	***IPeV***	***Metab***	***molMW***	***N&O***	***nonHatm***
CLOF	0.244	0.026	0.173	0.172	0.040	0.224
PHEN	0.532	0.020	0.076	0.580	0.474	**0.610**
	PercentAbs	***PISA***	***PSA***	***QPlogBB***	***QPlogHERG***	***QPlogKhsa***
CLOF	0.088	0.225	0.100	0.156	0.297	0.443
PHEN	0.161	0.534	0.505	0.064	**0.649**	**0.794**
	QPlogKp	***QPlogPC16***	***QPlogPoct***	***QPlogPo/w***	***QPlogPw***	***QPlogS***
CLOF	0.451	0.447	0.263	0.441	0.035	0.290
PHEN	**0.737**	0.427	0.261	**0.787**	0.187	**0.737**
	QPPCaco	***QPPMDCK***	***QPpolrz***	***ringatoms***	***Rotor***	***RuleOfFive***
CLOF	0.179	0.098	0.376	0.244	0.169	0.215
PHEN	0.384	0.026	**0.637**	0.532	0.070	0.516
	RuleOfThree	***SAfluorine***	***SASA***	***Stars***	***volume***	***WPSA***
CLOF	0.264	0.158	0.424	0.002	0.454	0.084
PHEN	0.502	0.009	**0.629**	0.593	**0.601**	0.001

accptHB Estimated number of hydrogen bonds that would be accepted by the solute from water molecules in an aqueous solution, ***ACxDN5SA*** Index of cohesive interaction in solids,. ***CIQPlogS*** Conformation-independent predicted aqueous solubility, in56 Number of atoms in 5- or 6-membered rings, ***CNS*** Predicted central nervous system activity on a −2 (inactive) to +2 (active) scale, ***dip-2/V*** Square of the dipole moment divided by the molecular volume, ***dipole*** Computed dipole moment of the molecule, ***donorHB*** Estimated number of hydrogen bonds that would be donated by the solute to water molecules in an aqueous solution, ***EA(eV)*** PM3 calculated electron affinity, ***FISA*** Hydrophilic component of the SASA (SASA on N, O, and H on heteroatoms), ***FOSA*** Hydrophobic component of the SASA (saturated carbon and attached hydrogen), ***glob*** Globularity descriptor, ***HumOrAbs*** Predicted qualitative human oral absorption: 1, 2, or 3 for low, medium, or high, ***in56*** Number of atoms in 5- or 6-membered rings, ***IP(ev)*** PM3 calculated ionization potential, ***Metab*** Number of likely metabolic reactions, ***molMW*** Molecular weight of the molecule, ***N&O*** Number of nitrogen and oxygen atoms, ***nonHatm*** Number of heavy atoms (nonhydrogen atoms), ***PercentAbs*** Predicted human oral absorption on 0–100% scale. ***PISA*** π (carbon and attached hydrogen) component of the SASA, ***PSA*** Van der Waals surface area of polar nitrogen and oxygen atoms, ***QPlogBB*** Predicted brain/blood partition coefficient, ***QPlogHERG*** Predicted IC50 value for blockage of HERG K+ channels, ***QPlogKhsa*** Prediction of binding to human serum albumin, ***QPlogKp*** Predicted skin permeability, log *Kp*, ***QPlogPC16*** Predicted hexadecane/gas partition coefficient, QPlogPoct Predicted octanol/gas partition coefficient, ***QPlogPoct*** Predicted octanol/gas partition coefficient, ***QPlogPo/w*** Predicted octanol/water partition coefficient, ***QPlogPw*** Predicted water/gas partition coefficient, ***QPlogS*** Conformation-independent predicted aqueous solubility, log *S*. *S* in mol dm^{-3} is the concentration of the solute in a saturated solution that is in equilibrium with the crystalline solid, ***QPPCaco*** Predicted apparent Caco-2 cell permeability in nm/sec, ***QPPMDCK*** Predicted apparent MDCK cell permeability in nm/sec, ***QPpolrz*** Predicted polarizability in cubic angstroms, ***Ringatoms*** Number of atoms in a ring, ***rotor*** Number of non-trivial (not CX3), non-hindered (not alkene, amide, small ring) rotatable bonds, ***RuleOfFive*** Number of violations of Lipinski's rule of five, ***RuleOfThree*** Number of violations of Jorgensen's rule of three, ***SAfluorine*** Solvent-accessible surface area of fluorine atoms, ***SASA*** Total solvent accessible surface area (SASA) in square angstroms using a probe with a 1.4 Å radius, ***stars*** Number of property or descriptor values that fall outside the 95% range of similar values for known drugs, ***volume*** Total solvent-accessible volume in cubic angstroms using a probe with a 1.4 Å radius, ***WPSA*** Weakly polar component of the SASA (halogens, P, and S). Cells reporting a $r^2 \geq 0.6$ are shaded and the relative correlation coefficients are reported in bold.

site the regions where certain chemical groups can interact favourably [35].

AutoDock 4.2 [32] was chosen as docking tool, having proved its ability to consistently reproduce the pose experimentally observed in the PPARγ/**1b** with a RMSD of 1.2 Å. The PPARα structure was then superimposed on PPARγ and affinity maps were calculated by AutoGrid, using a box 55 × 65 × 55 centred on the Cartesian coordinates of **1b** with a spacing of 0.375 Å. For each compound 100 runs of docking were carried out, exploring the conformational space with the Lamarckian Genetic Algorithm (LGA). From each

Table 3
$pA_{PPAR\gamma}$ r^2 values of the QikProp descriptors for **CLOF** and **PHEN** classes.

$pA_{PPAR\gamma}$	***accptHB***	***ACxDN5SA***	***CIQPlogS***	***CNS***	***Dip2V***	***dipole***
CLOF	0.003	0.021	**0.891**	0.000	0.024	0.211
PHEN	**0.633**	**0.736**	**0.862**	0.444	0.094	0.058
	donorHB	***EAeV***	***FISA***	***FOSA***	***glob***	***HumOrAbs***
CLOF	0.000	0.142	0.023	0.106	0.590	0.358
PHEN	0.280	0.041	0.391	0.192	0.596	0.160
	in56	***IPeV***	***metab***	***molMW***	***N&O***	***nonHatm***
CLOF	**0.773**	0.012	0.139	**0.734**	0.004	**0.893**
PHEN	0.585	0.029	0.003	**0.699**	**0.779**	**0.627**
	PercentAbs	***PISA***	***PSA***	***QPlogBB***	***QPlogHERG***	***QPlogKhsa***
CLOF	0.471	0.516	0.019	0.050	**0.624**	**0.810**
PHEN	0.213	**0.614**	0.565	0.136	**0.722**	**0.843**
	QPlogKp	***QPlogPC16***	***QPlogPoct***	***QPlogPo/w***	***QPlogPw***	***QPlogS***
CLOF	0.523	**0.675**	**0.905**	**0.887**	0.451	**0.789**
PHEN	**0.695**	0.429	0.321	**0.875**	0.172	**0.881**
	QPPCaco	***QPPMDCK***	***QPpolrz***	***ringatoms***	***rotor***	***RuleOfFive***
CLOF	0.016	0.003	**0.868**	**0.773**	0.007	**0.728**
PHEN	0.352	0.121	**0.652**	0.585	0.004	0.484
	RuleOfThree	***SAfluorine***	***SASA***	***stars***	***volume***	***WPSA***
CLOF	**0.766**	0.000	**0.821**	0.406	**0.869**	0.003
PHEN	0.286	0.049	0.598	0.479	0.552	0.045

For descriptors see Table 2. Cells reporting a $r^2 \geq 0.6$ are shaded and the relative correlation coefficients are reported in bold.

AutoDock output file, the most populated cluster with the lowest energy binding mode was chosen, and same selected pose taken into account in the consequent 3D-QSAR study.

Potency data were related to the recently introduced GRID independent descriptors (GRIND) [36] calculated through ALMOND 3.3.0 on a 0.5 Å spaced grid defined around the ligands using the hydrophobic (DRY), hydrogen bond acceptor (HBA), donor (HBD) and shape (SHP) probes. With this latter probe the local curvature of the surface (a property highlighting the substituents protruding from the skeleton of the molecule) is introduced [37]. From the MIFs original matrix a maximum number of 200 nodes were extracted for the original data matrix resulting into 510 and 530 independent variables for both PPARα and PPARγ models, respectively. PLS analyzes were performed using default settings. No initial scaling was applied to the original X-variable matrix, which was subsequently filtered by Fractional Factorial Design run to select the not redundant and really significant variable. Cross-validation was performed using the *leave-one-out* (LOO) procedure to select the optimal number of components in the PLS model equal to a significant increase of the cross-validation coefficient q^2 (at least 5%). For sake of clarity, the variables are coded reporting the probes used in the GRIND calculation and a sequential number from which, according to the default grid spacing (0.5) and a smoothing factor (0.8), the distance between the nodes where field effects are measured, is obtained.

2.2. Mutagenesis

The expression plasmids for PPARα-LBD and PPARγ-LBD fused in frame with the Gal4 DNA binding domain (pGal4-PPARγ-LBD) and the reporter vector containing five copies of the Gal4 upstream activating sequences (pGal4UAS-Luciferase) driving the transcription of the luciferase reporter gene were kindly donated by Dr. Krister Bamberg (AstraZeneca, Mölndal, Sweden). The mutants PPARα A454M, and PPARγ M463A were prepared using the QuikChange site-directed mutagenesis kit (Stratagene, La Jolla, CA) [24] and confirmed by automated sequencing. pCMV-GFP, containing the *GFP* gene driven by the cytomegalovirus early promoter/enhancer (Clontech, Mountain View, CA), was used as an internal standard to normalize for transfection efficiency across wells. For transactivation assays, HepG2 cells (HB-8065, American Type Culture Collection, Manassas, VA) were transfected in suspension with 30 ng of pUAS5XGal4-Luc reporter vector, 30 ng of receptor expressing vector, 2 ng of pCMV-GFP as an internal standard for transfection efficiency to a total of 62 ng of DNA per well, using Lipofectamine® 2000 (Invitrogen) as a transfection reagent [24]. Transfected cells (2×10^4/well) were then seeded in 96-well plates. Six hours after transfection cells were treated with the indicated compounds in Dulbecco's Modified Eagle Medium, (Invitrogen, Milano, Italy) containing 100 U penicillin G $\times$ mL^{-1}, 100 μg of streptomycin sulphate $\times$ mL^{-1} and 10% charcoal stripped foetal bovine serum (Euroclone, Milano, Italia). Green Fluorescence Protein intensity was assessed by bottom reading of the plated living cells. Then luciferase activity in cell extracts was determined after 16 h with a luciferase detection kit (Perkin Elmer, Monza, Italia) using a plate reader luminometer (Envision, Perkin Elmer). Transfection experiments were performed in quadruplicate and repeated at least three times.

3. Results and discussion

The ability of twenty-two previously synthesized chiral dual PPARα/PPARγ agonists was modelled in this study according to the following protocol:

1. structural characterization of the binding sites based on the crystal structures of the two different PPAR isoforms;
2. classical quantitative structure–activity relationship based on bidimensional descriptors (2D-QSAR);
3. docking of the agonists into the PPARα and PPARγ binding site;
4. chemometric analysis of biological activity on three-dimensional basis (3D-QSAR) and development of pharmacophore models for the observed PPARα/PPARγ selectivity.

3.1. SAR study of dual PPAR agonists

The compound data set was grouped into three different classes: clofibric acid (**CLOF**), phenylacetic acid (**PHEN**), and 2-(naphthalenyl-2-oxy)acetic acid (**NAPH**) derivatives. Structures and related activities, expressed as pA, are reported in Table 1. Biological data are referred only to the (*S*) isomers since from our previous studies [16–19] the pivotal role of enantioselectivity clearly came out, being in most cases the (*R*) enantiomers much less powerful towards both PPARα and PPARγ. A valuable complement to this evidence has been also given by the X-ray structure of the PPARγ-**1b** complex where an unambiguous positioning of the (*S*) enantiomer was observed. This ligand occupies a branch of the PPARγ LBD, named *diphenyl pocket* (*DPP*) which is substantially different from the *benzophenone pocket* (*BPP*), a contiguous region of the hydrophobic pocket formed by H3, H7, and H11, occupied by some known ligands (i.e. thiazolidinediones and glitazones) and also by the (*R*) enantiomer of **1b** [22]. It has been postulated that the interactions occurring at the *DPP* might cause some structural changes in the region comprising H3, H11, H12 and the loop 11/12 with consequent increase of RXR recruitment and activation of target gene transcription [24]. As long as these data were concerned, we decided to model the PPARα/γ pharmacological profile only for the (*S*) enantiomers.

Structure–activity relationship for **CLOF** derivatives suggested that PPARα activity slightly increases with the length of the bridge linking the chiral centre to the unsubstituted phenyl ring. In fact, compounds **1a**, **2a**, and **10a** have a comparable activity value (pAα = 5.41–6.23), while the introduction of a long aromatic pendant at the para position of the phenyl significantly affects PPARγ activity (cfr. compounds **6a**, **7a**, **8a** and **10a**). Interestingly, the presence of a phenoxy ring results in the greatest PPARγ selectivity (ΔpA = 1.51 logarithmic units), while the isosteric substitution of a methylene group with oxygen does not affect either pA values (cfr. compounds **1a** and **4a**, pAα = 5.62 vs 5.60 and pAγ = 5.15 vs 5.78).

For **PHEN** derivatives the introduction of functional groups with a certain hindrance in the para position of the phenoxy ring increases activity on both receptor subtypes, with a larger effect on selectivity towards α, as demonstrated by **2b** (pAα = 7.96 and pAγ = 6.24). In contrast, polar substituents (i.e. hydroxymethyl group for compound **5b**) drop deeply the activity on both receptor subtypes (pAα = 4.54 and pAγ = 4.59). Similarly, activity decreases with small substituents such as chlorine (**10b**). Finally, electron releasing groups like methoxy (**8b**), proved to affect the selectivity quite appreciably (pAα = 5.60 vs pAγ = 4.70).

For **NAPH** no selectivity was observed, nevertheless it has to be pointed out that from the SAR these derivatives no significant inferences can be formulated due to the limited number of compounds populating this class.

3.2. Structural features of PPARs and LBD mapping

In order to investigate the properties of our targets, and to evince then some rules underlying binder selectivity, we investigated the structural features of both PPARs. Not surprisingly, an

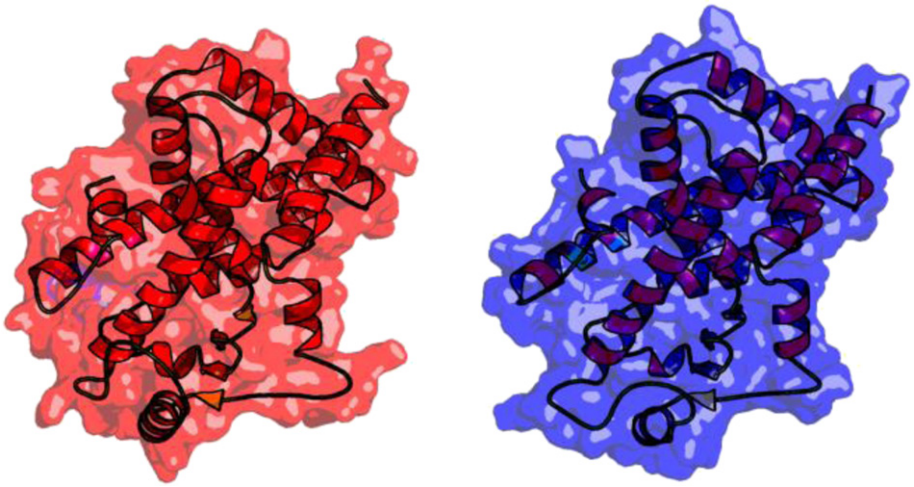

Fig. 1. X-ray three-dimensional structure of PPARα (red, PDB code 2REW) and PPARγ (blue, PDB code 3B3K). The solvent accessible surfaces are displayed. (For interpretation of the references to colour in this figure legend, the reader is referred to the web version of this article.)

extremely large (>60%) degree of similarity characterizes the two receptor subtypes, and therefore the folding over the whole polypeptide chain is highly preserved (Fig. 1). So it might be expected that the different potency measured within the pA data set should be a consequence of a mere variation in the primary sequence of the two subtypes.

Due to this evidence, we decided then to describe the main properties of PPARs LBDs in terms of chemical fingerprints calculating the MIFs on the solved X-ray structures and trying, at the same time, to assess the main forces which most likely govern the receptor–ligand recognition process.

In this view, the DRY, C3 and O probes (reported according to the GRUB definition) were selected to weight and describe, respectively, the hydrophobic, steric, and polar effects mainly occurring on the previously mentioned *DPP*. As it can be perceived from Fig. 2, C3 seems to be the most relevant in discriminating ligand selectivity towards PPARα/γ. Indeed, the MIFs calculated with this probe highlighted in both receptors subtypes favourable interaction areas with similar location, but different extension, with a much more large cleft in the α than γ subtype. In particular, the C3 probe draws a more hindered area in PPARγ, suggesting therefore a greater steric accessibility in PPARα.

A plausible explanation for this different accessibility might be ascribed to a single amino acid on the loop 11/12: as it might be noticed in the relative sequences alignment, Ala454 of PPARα corresponds to Met463 in PPARγ (Fig. 3) and, as long as the difference of the two side chains is acknowledged, it cannot be excluded that Met463 might acts as a "lid" in PPARγ limiting, or even hampering, the accessibility to the LBD for agonists bearing bulky substituents.

The same kind of occurrence was not observed countering the MIFs of the other two probes, assessing therefore the main role of binding accessibility and steric hindrance on the regulation of the PPAR selectivity.

3.3. 2D-QSAR of dual PPARs

In order to rationalize the evidences highlighted by SARs and binding site mapping, and to investigate the molecular determinants defining the pharmacological profile of **CLOF**s and **PHEN**s, a 2D-QSAR study was carried out, and both mathematical

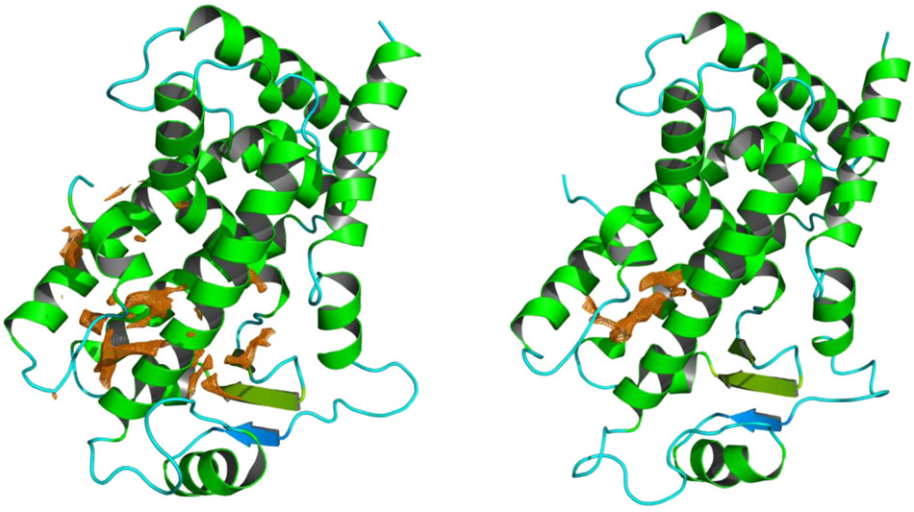

Fig. 2. Molecular interaction field, measured with the C3 probe in the PPARα (left) and PPARγ (right) binding site. Maps are calculated on a 0.25 Å spaced grid and plotted at a counter level of 3 kcal·mol^{-1}.

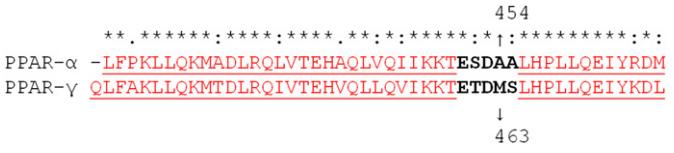

Fig. 3. Sequence alignment of PPARα and PPARγ H11-H12 and loop 11/12. Underlined residues comprise the helices, bold ones represent the loop.

and regression models were developed. In this part of the study, the **NAPH** compounds **1c** and **2c** were not evaluated aiming to deal only with highly congeneric series.

Starting from the twenty **CLOF** and **PHEN** analogues, fifty mono and bidimensional descriptors included in the QikProp software package were calculated. These descriptors are numerical variables or properties that can be calculated from the single atomic matrix of connections, and not by the atomic coordinates, and they are therefore independent conformations. The correlation coefficients between pAs and QikProp descriptors are reported in Tables 2 and 3.

For PPARα, no significant relationships ($r^2 < 0.5$) were found within the **CLOF** data set, probably due to the low pA range. On the contrary, the activity endowed by **PHEN**s showed a good correlation with the water/octanol partition coefficient (*QPlogPo*/w), explaining almost 80% of the observed data variance, as reported in the following Equation (1):

$$pA\alpha = 0.850(\pm 0.147)QPlogPo/w - 2.138(\pm 0.688) \quad (1)$$

$$n = 11;\ r^2 = 0.787;\ s = 0.463;\ F = 33.295$$

Equation (1) shows a positive modulation of the activity given by lipophilicity, as outlined by the sign of *QPlogPo*/w coefficient; this might suggest that in the case of **PHEN** derivatives, the higher the lipophilicity the better should be the agonism towards PPARα (a similar parabolic, rather than linear, correlation was also found). Further valuable ($r^2 > 0.7$) correlations between the biological activity and other variables (i.e. *CIQPlogS*, *QPlogKhsa*, and *QPlogS*) were not taken into account. These variables are indeed most likely related to pharmacokinetics, rather than pharmacodynamics aspects, and therefore they are less suitable in the interpretation of the performed biological tests.

For PPARγ a good regression model, with even a better statistical significance as expressed by higher *F* values, was also obtained with the *QPlogPo*/w descriptor for both class of compounds (see Eqs. (2) and (3)). However, for **PHEN**s a lower coefficient was gained, likely suggesting a less important effect of the hydrophobic interactions for this class of derivatives.

$$pA\gamma = 1.357(\pm 0.17)QPlogPo/w - 0.665(\pm 0.89) \quad (2)$$

$$n = 10;\ r^2 = 0.887;\ s = 0.287;\ F = 62.508$$

$$pA\gamma = 0.607(\pm 0.07)QPlogPo/w - 2.843(\pm 0.36) \quad (3)$$

$$n = 11;\ r^2 = 0.875;\ s = 0.241;\ F = 62.940$$

Further differences between pAα and pAγ might be observed evaluating effects encoded by other descriptors, as shown by the regression models achieved with *SASA*, *volume*, and *dipole* descriptors. In fact, regression models with the aforementioned descriptors showed much better statistical figures for pAγ than pAα, especially for **CLOF**s (*SASA* $r^2 = 0.821$ vs 0.424; *volume* $r^2 = 0.869$ vs 0.454; *QPpolrz* $r^2 = 0.868$ vs 0.376). In contrast, the same descriptors expressed almost identical correlations or even less significant for **PHEN**s (*SASA* $r^2 = 0.598$ vs 0.629; *volume* $r^2 = 0.552$ vs 0.601; *QPpolrz* $r^2 = 0.652$ vs 0.637).

Afterwards, two variable regression models were developed and the following regressions were obtained for **CLOFs** (Eqs. (4) and (6)) and **PHENs** (Eqs. (5) and (7)), respectively.

$$pA_{PPAR\alpha} = 0.003(\pm 0.009)Vol + 0.007(\pm 0.003)FOSA + 2.323(\pm 0.88) \quad (4)$$

$$n = 10;\ r^2 = 0.717;\ s = 0.206;\ F = 8.849$$

$$pA_{PPAR\alpha} = 0.011(\pm 0.003)SASA - 0.044(\pm 0.014)PSA + 2.192(\pm 2.114) \quad (5)$$

$$n = 11;\ r^2 = 0.830;\ s = 0.439;\ F = 19.597$$

$$pA_{PPAR\gamma} = 1.271(\pm 0.143)QPlogPo/w + 0.166(\pm 0.072)dipole - 0.767(\pm 0.718) \quad (6)$$

$$n = 10;\ r^2 = 0.936;\ s = 0.231;\ F = 50.853$$

$$pA_{PPAR\gamma} = 0.005(\pm 0.001)SASA - 0.920(\pm 0.136)N\&O + 5.385(\pm 0.996) \quad (7)$$

$$n = 11;\ r^2 = 0.939;\ s = 0.177;\ F = 62.471$$

The models were not so relevant for both **CLOFs** and **PHENs** acting as PPARα agonists, as suggested by low *F* values. Interestingly, there is a better statistics in the correlation of pAγ with two QikProp terms. Indeed, for **CLOF**s, *dipole* increased the correlation with PPARγ activity, suggesting then a partial, but positive, modulation of the pharmacological profile ascribable not only to hydrophobic elements but also to other chemical features or functional groups which enhance the polarization of the agonist scaffold. On the contrary Equation (7) shows for **PHEN**s a negative control in the PPARγ activity by the *N&O* descriptor, encoding the molecular polarity with the presence of nitrogens and oxygens, as already highlighted by SAR. Therefore, in this latter case, electronegative atoms might be detrimental for receptor interactions.

This first study showed that the selected set of derivatives might be a useful tool to correctly interpret the biological data through a series of 2D-QSAR equations. To further prove this, the observed compounds potency and selectivity were further interpreted by means of three-dimensional studies (3D-QSAR and docking), as described in the next sections.

3.4. Docking studies

More than one hundred X-ray crystal structures of PPARs LBD have been already solved: the majority are complexes of the γ subtype with diverse type of binders while very few match the α one. Nonetheless, the amount of information concerning the structural features of our targets is as much as necessary to satisfactorily support a structure-based ligand study aimed to a better definition of the chemical and structural motifs dominating over the activity and selectivity endowed in the **CLOF**, **PHEN** and **NAPH** analogues.

In all the docked agonists an extremely conserved binding mode, in large agreement to the crystallographic data achieved for **1b**, was attained in both PPARα and PPARγ structures. In details, a kind of inverted Y pose was noticed, with the negatively charged carboxylic group pointing towards a pool of polar residues, and two hydrophobic pendants, pointing one towards the *BPP* and the second filling the *DPP* between of H3, H11 and H12.

These observations might be better perceived from the dockings of **6a** and **2b**, the most active and selective agonists for PPARα and PPARγ, respectively, reported in Fig. 4.

In detail, **2b** and **6a** dockings both show the carboxylic group making several hydrogen bonds with conserved polar residues namely, Tyr314, His440 and Tyr464 for PPARα, Ser289, His323, Tyr327 and His449 for PPARγ. As also observed from X-ray data, this network is essential to ensure the correct anchorage of the ligand to the binding site, and then a proper stabilization of the ligand–receptor complex in both receptor subtypes.

As long as this is concerned, dockings helped to interpret the PPAR specificity of ligands: the long hydrophobic tail of the most active and selective PPARα agonist **2b** is deeply buried into the *DPP*, making extensive and favourable hydrophobic contacts with the benzyl group surrounded by aromatic or aliphatic residues like Phe273, Phe351, Ala454 and Leu456. The same evidence cannot occur for **6a**, bearing a lone chlorine atom in the same position of the ligand scaffold (data not shown). It is helpful to remind that the previously binding site mappings carried out for PPARα reported a wider accessible moiety comprising the *DPP*, and that the 2D-QSAR study showed a good correlation with lipophilicity only for **PHENs** and not for **CLOFs**.

It is very worth noting that Ala454 is part of the loop 11/12, and it might be therefore an extremely important hot spot residue because H12 modulates, by its movements and extension, the interaction with the activating factor recruited by PPAR once it binds to DNA. Moreover, as previously highlighted by the binding site mapping, the PPARα surface moiety is more wide open and accessible to ligands bearing on the molecular scaffold bulkier or sterically hindered substituents as in the case of **2b**. On the contrary, the different pharmacological profile of **6a**, which is more active and selective towards PPARγ, might be due to the presence on the same loop of Met463, which replaces the alanine in the α isoform. As already assessed before, this mutation might result into a more occluded hydrophobic cavity for accommodating compounds with a larger pendant moiety. This hypothesis is supported by Equation (6), which highlights a considerable role for the *dipole* molecular descriptor.

An additional significant difference between the two targets is one residue mutation occurring on H3, where Thr279 of PPARα is replaced by Arg288 in PPARγ. This suggests that in the former instance the ligand–receptor complex is mainly stabilized by polar bond such as hydrogen bonds, while in the latter a charge–transfer complex might take place. This evidence might be perceived from the docking of **6a**, where the long aromatic tail is pointing towards the flexible side chain of Arg288. It has to be pointed out that, regardless what displayed in Fig. 4, the electron density map suggests for this residue also an alternative side chain location facing the inner part of the ligand binding site [22]; this might be a plausible interpretation of the higher PPARγ selectivity measured for **CLOF** derivatives bearing at the para position larger substituents.

A further validation of dockings is finally given by the significant correlations between the binding free energy and pA values found within each congeneric series. Excluding in just some instances a single outlier, namely compound **2a** and **9b** for PPARα and

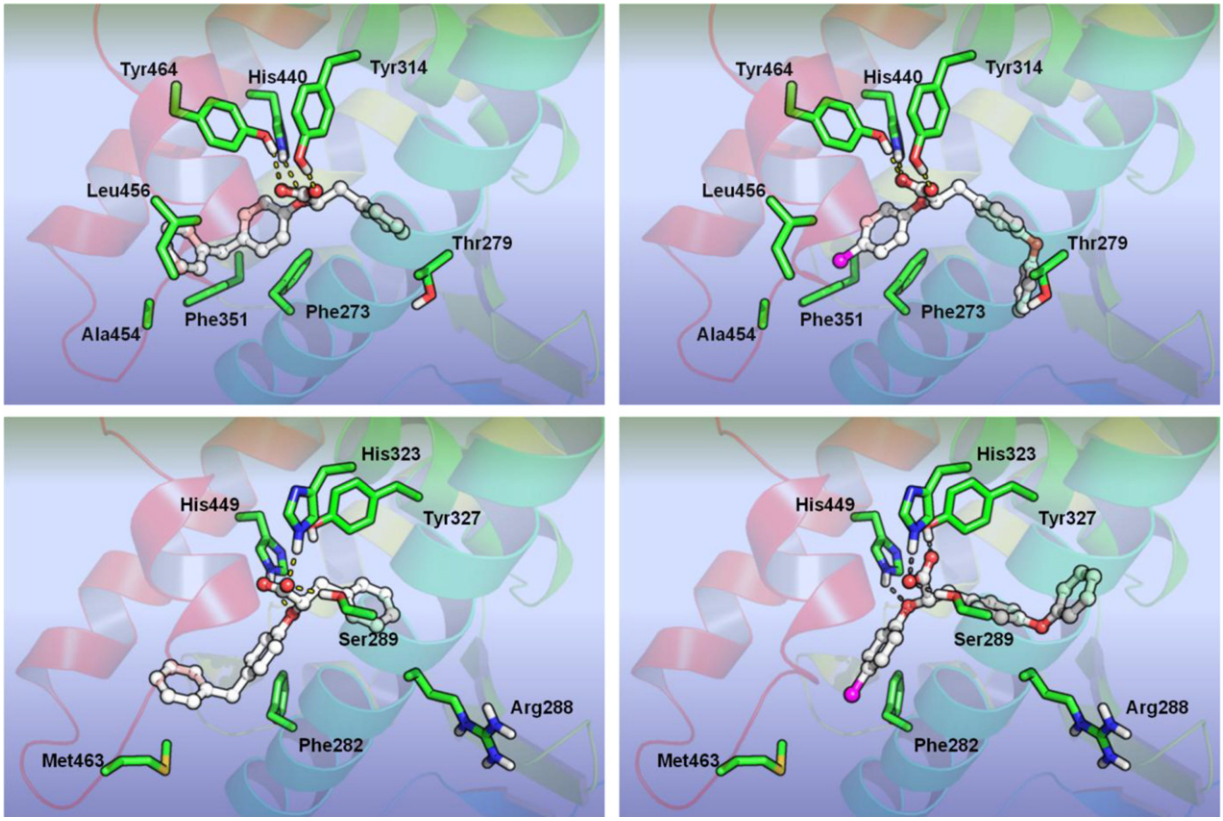

Fig. 4. Docking of the compound **2b** and **6a** respectively in the PPARα (top, right and top, left) and PPARγ (bottom, left and bottom, right) binding site. The estimated free energy of binding are −7.48 and for −9.49 kcal·mol^{-1} for compound **2b**, −7.60, and −9.12 kcal·mol^{-1} for compound **6a**.

compound **4b** for PPARγ, good correlations (r^2 = 0.638–0.840) were gained. Even if the AutoDock scoring function is calibrated on some empirical parameters most likely able to reproduce affinity (i.e. pK_i), rather than efficacy (i.e. pA), biological data [38,39].

Docking study also allowed us to formulate crude pharmacophore hypothesis interpreting the activity of our agonists together with the identification of some molecular determinants or structural elements (i.e. Ala454/Met463 of the loop 11/12) highly important for the observed selectivity.

3.5. 3D-QSAR

To validate the insights obtained by 2D-QSAR and dockings on the main structural requirements for an effective binding to the receptor, and depict a pharmacophore model, a comprehensive chemometric analysis was performed. This assignment was completed, for all the analyzed agonists, calculating three-dimensional molecular descriptors able to adherently describe some binder properties, also according to ligand shape.

In 3D-QSAR analysis, molecular descriptors are intended as force fields measured on three dimensional structure, using appropriate probe atoms. These descriptors are then compared on the basis of their intensity and on the surface where a greater variance of the effect of field, encoded by these descriptors, is measured. Consequently, molecular alignment is very important; there should be a consensus of the molecule shape in the space, and the selected conformations should match the bioactive ones.

Interestingly, GRINDs are a particular set of molecular descriptors which, independently from the alignment of the ligands, describe, in terms of intramolecular distances, the link between chemical features of functional groups characterizing each agonist and their biological activity. Basically, GRINDs rely on the definition of a virtual binding site, and at the same time embody the geometrical relationship between hot spot residues of a receptor cavity. In other words, through using these three-dimensional descriptors, information contained in the MIF is transformed, generating a set of variables that are independent from the position of the molecules in the Cartesian and chemical space. Nonetheless, even though Almond results have proved to be not affected by likely unacceptable molecular superposition, agonist binding poses obtained from previous dockings were selected as alignment rules in this step.

The procedure used can be summarized as follows: fields are filtered involving only the nodes that have lower energy values, representing the most favourable interactions, and nodes located far away between each other, in order to represent the molecule in its full extension. At this point the product of the interaction energies between the first pair of nodes is computed. From the data in Table 4 the quality of this approach might be valued.

Interestingly, robust models with valuable statistical figures were obtained: good correlation coefficient values (PPARα $r^2 = 0.942$; PPARγ $r^2 = 0.891$) reflecting a good compliance between predicted and experimental data, as well as high cross-validation correlation coefficients ($q^2 > 0.740$).

Table 4
Statistical results of PLS analysis for **CLOF**, **PHEN** and **NAPH** compounds.

	n[a]	Var[b]	r^2 [c]	q^2 [d]	s[e]	ONC[f]
PPARα	22	337	0.942	0.743	0.170	3
PPARγ	22	350	0.891	0.744	0.263	2

[a] Number of analyzed compounds.
[b] Number of the descriptors (variables) obtained after one phase of FFD.
[c] Correlation coefficient.
[d] Cross-correlation coefficient by the LOO method.
[e] Standard deviation.
[f] Number of latent variables.

A better interpretation of these statistical models is provided by the PLS coefficients plots related to the different probes, where it is possible to perceive, depending on the sign, the GRINDs most likely affecting the receptor activation (see in Fig. 5). Variables with positive coefficients are those that positively influence the interaction of the agonist with its target, hence the greater the value the higher the pA. In contrast, the negative coefficients indicate those variables that are unfavourable, and bring thus to a consequent lowering of the measured activity.

The comparison of the two graphs of PLS coefficients shows that DRYDRY variables, determined by autocorrelation of hydrophobic fields, seem to be more important in the PLS PPARα model than in PLS PPARγ one, where instead a negative modulation is given by auto correlated HBD variables. DRY variables positively modulate the agonism towards both PPARα and PPARγ in concert with shape effects (DRYSHP), while the same effects, if auto correlated, resulted in a different modulation of pA, negative for PPARα and positive for PPARγ.

As mentioned, these variables indicate which chemical and physical properties of a specific ligand correlate better with the biological activity, and also indicate the exact distance in three dimensional space where field effects, encoding the same type of forces, are observed and measured. In this way we formulated a sound, statistical based, pharmacophore hypothesis interpreting the observed data variance, which represents not only functional groups important for good activity, but especially the distance best fitting the same groups or pairs of atoms.

A better understanding might be achieved by the graphical display of GRID filtered nodes relative to the mentioned interactions: indeed, for PPARα the representation of the highest positive coefficient variable DRYDRY-39, reported in Fig. 6 with the most active and selective compound **2b**, demonstrated that hydrophobic interactions, probably related to the π–π stacking phenomena, are important once occurring at an optimal distance equal to 15.6 Å. On the contrary, variable DRYSHP-47 suggested that a further agonism might be gained placing in the ligand skeleton an aromatic ring at greater distance (18.8 Å) from a second element, most likely the para aromatic carbon, able to induce a local curvature and protruding from the molecular scaffold. 2D-QSAR analysis and docking formerly suggested for the highly active compound **2b** a positive role for the interaction with the receptor of non polar interactions and of lipophilic substituents elongating the binder extension, as consequence of the structural motif of the loop 11/12 discriminating PPARα.

On the other hand, variables SHPSHP-28, and also HBDSHP-40, indicate for the low activity compound **5b** a negative modulation of pA for distances measured between the nodes equal to 11.2 Å and 16.0 Å. A plausible interpretation is hold by the structural difference between compounds **5b** and **2b**. The phenoxy ring of the most active agonist **2b** is bearing a large and hydrophobic substituent (i.e. benzyl) while the less active **5b** carries a smaller and polar one (i.e. hydroxymethyl). So a negative modulation of the activity is almost certainly observed with interactions associated with the shape and hydrophobic effects occurring at short distances. This suggests that in the rational design and synthesis of future compounds, elongated portions that can be functionalized with hydrophobic moieties should be preferred over tiny and electronegative cliché.

In the PPARγ PLS model the variables with the highest positive coefficient are SHPSHP-46 and DRYSHP-42, reported in Fig. 6 together with the most active agonist **6a**. These variables, encoding a node distance respectively equal to 18.4 Å and 17.4 Å, show the presence of favourable, which mimic the two pendant moieties resembling the inverted-Y binding mode previously described in the docking section.

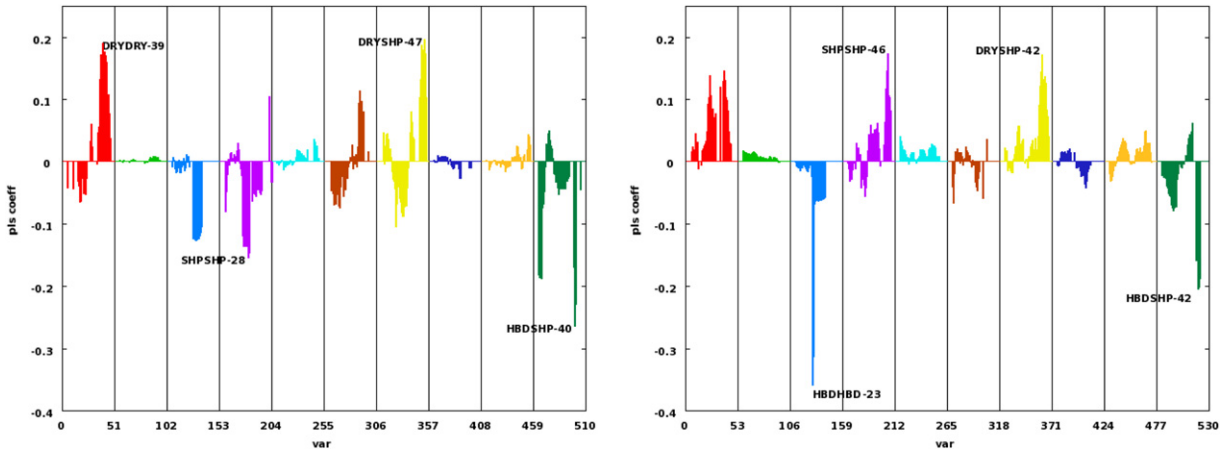

Fig. 5. Coefficients plots for PPARα (left) and PPARγ (right) PLS models. The most relevant positive and negative variables are highlighted (see text).

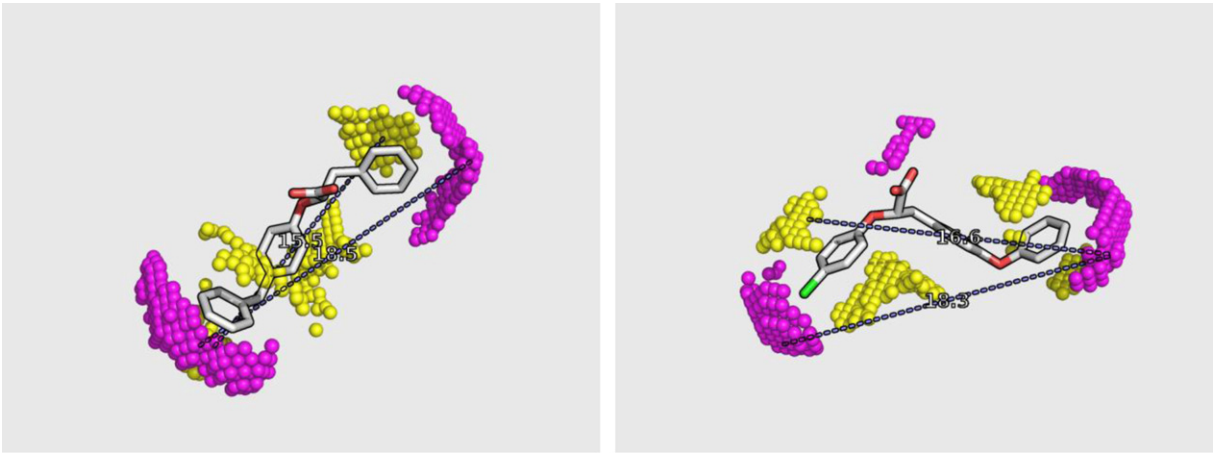

Fig. 6. Grid filtered fields for PPARα (left) variables DRYDRY-39 and DRYSHP-47 and PPARγ (right) variables SHPSHP-46 and DRYSHP-42 (code colours = DRY yellow, SHAPE magenta). Dashed lines connecting grid nodes, positively affecting the pA of compounds **2b** and **6a**, and their relative distances are also depicted to help interpretation. (For interpretation of the references to colour in this figure legend, the reader is referred to the web version of this article.)

It is interesting to note that the Y is less symmetrical in PPARγ than in PPARα model. This greater ligand extension from one side, orientated towards the *BPP*, perhaps is induced by the Met463 on loop 11/12, impeding the presence of voluminous portions on both sides of the structure of the agonists.

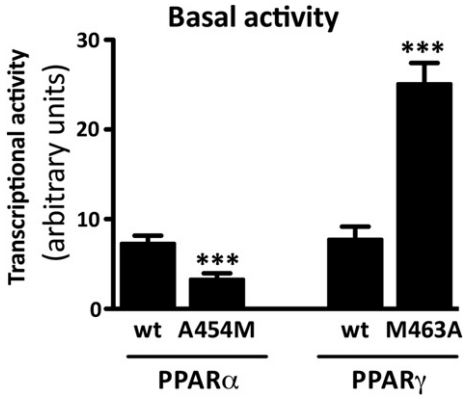

Fig. 7. Basal receptor activity of wild type and mutated PPARα and PPARγ in HepG2 cells. Values are calculated as percentage of maximum effect obtained with reference ligands (i.e., Wy14,643 for PPARα and rosiglitazone for PPARγ) represent the mean ± SD of three independent experiments each performed in quadruplicate.

On the other hand, as well as in the PPARα model, even in this case the more negative coefficients are related to polar interactions. In fact, the variables HBDHBD-23 and HBSSHP-42 for the less active PPARγ agonist **5b** indicate that the presence of hydrogen bond acceptor groups placed at 9.2 Å or 16.8 Å from the end of the molecule, is a negative factor reducing the value of pA.

3.6. Molecular determinants for PPAR selectivity

From the binding pose of the most active and selective PPAR agonists **6a** and **2b** we were finally able to sketch a pharmacophore interpreting the observed receptor selectivity. This depiction was done measuring in the three-dimensional space the distance between the functional groups of the aforementioned compounds, as validated by docking and chemometric analysis.

For an effective PPARα agonism a negative charged bit (i.e. a carboxylic group) must be spaced from a phenyl ring centroid, occupying the *DPP*, by almost 7.5 Å, taking the aromatic centroid as reference, being the same ring at almost 12.4 Å from the para carbon of a non substituted benzene, pointing towards the *BPP*. The distance of this same spot from the ionized moiety should be measured around 6.3 Å. On the contrary, PPARγ agonism should be gained if an unsubstituted phenyl ring is at bigger (almost 8.4 Å) distance from the negatively charged functional group.

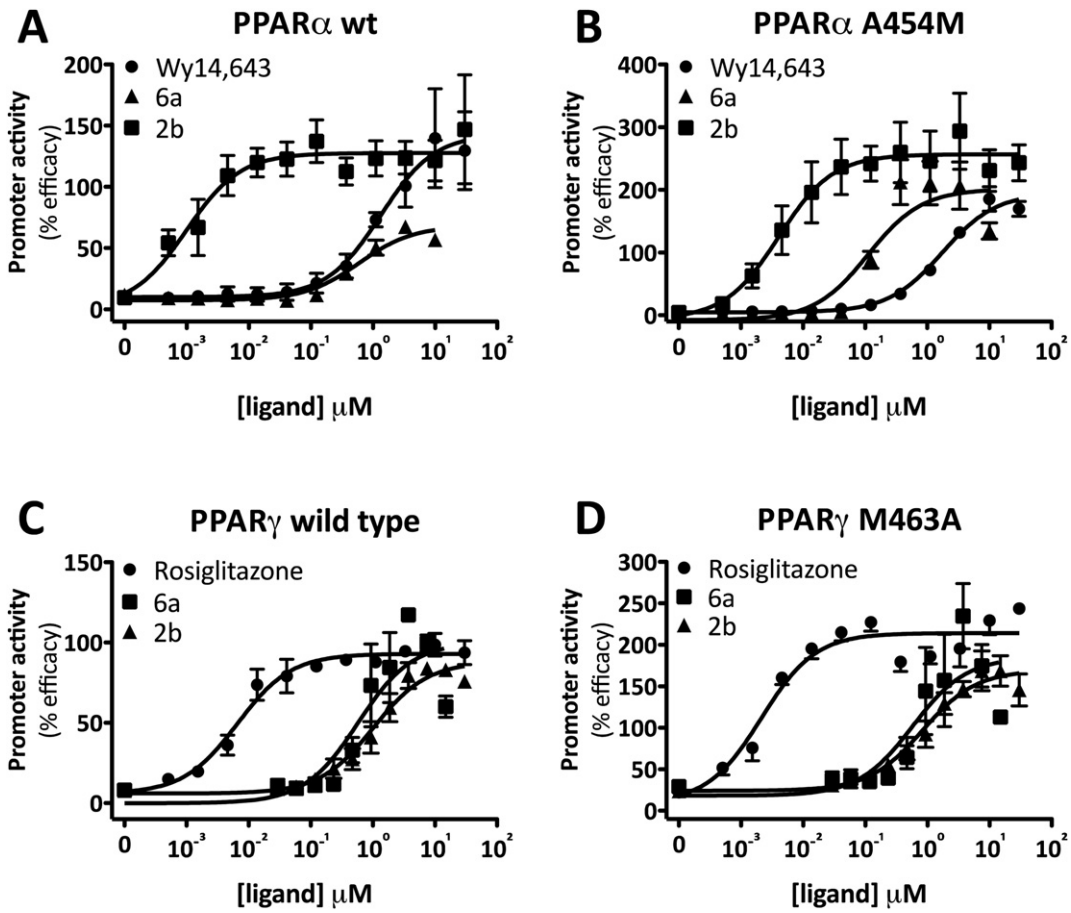

Fig. 8. Concentration-response curves of **2b** and **6a** with wild type and mutated PPARα (A, B) and PPARγ (C, D). The curves are expressed as percentage of maximum effect obtained with reference ligands Wy14,643 (PPARα) and rosiglitazone (PPARγ) and represent the mean ± SD of three independent experiments each performed in quadruplicate.

Moreover, a para substituent into the *DPP*, 7.6 Å away from an acid group and 13.6 Å away from an aromatic ring pointing to the *BPP*, might shift the selectivity towards PPARγ. The above observations are reported in the Chart 1, which summarizes the proposed hypothesis.

3.7. Site directed mutagenesis experiments

To perform site directed mutagenesis experiments, we focused our attention on the Ala454 and the corresponding residue, Met463, of alpha and gamma receptor isoform respectively. These amino acids are located on the loop 11/12 at the base of the DPP hydrophobic cavity, limiting the access of ligands in this region of the receptor in particular for the gamma isoform. A specific conformation of the H12 and the interactions occurring in the region comprising H3, H11, and the loop 11/12 is responsible for the recruitment of activating co-factors required for transcriptional activity in both receptor isoforms as previously reported [24]. Moreover is possible to assume that the mutation of these residues significantly interfere with the mechanism of receptors transcriptional activity.

The cell-based transcription assays performed in HepG2 cells confirmed the importance for the interaction with ligands of the amino residues in PPARs LBD identified from our docking and QSAR studies, and very intriguingly mutations resulted in a specular effect on the receptor basal activity.

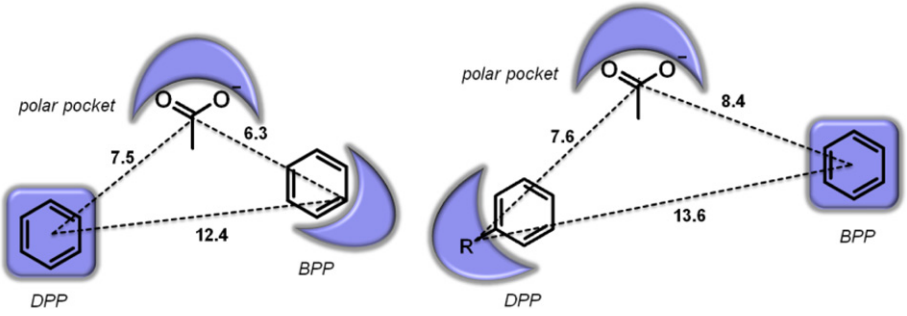

Chart 1. Proposed pharmacophore models for selective PPARα (left) and PPARγ (right) agonism.

Table 5
Potency of ligands with wild type and mutated PPARs is expressed as EC_{50} (μM).

Receptor	Wy14,643	Rosiglitazone	2b	6a
PPARα wt	3.46 ± 1.23	–	0.04 ± 0.02	3.9 ± 1.1
PPARα A454M	7.1 ± 2.1	–	0.4 ± 0.5	0.9 ± 0.03
PPARγ wt	–	0.01 ± 0.003	0.60 ± 0.18	0.32 ± 0.14
PPARγ M463A	–	0.002 ± 0.001	0.47 ± 0.17	0.34 ± 0.12

Values were calculated from three independent experiments and are expressed as mean ± SD.

Concerning PPARα, the mutation A454M yielded a decrease in the basal receptor activity, while PPARγ M463A significantly enhances the same activity (Fig. 7).

The potency of Wy14,643 and **2b**, PPARα selective agonist and about 100 times more potent than the reference, was lower with the mutated PPARα A454M as compared to wild type PPARα while that of **6a**, the PPARγ selective agonist, was significantly higher (Table 5 and Fig. 8A and B). Conversely, the mutation M463A increased the basal receptor activity of PPARγ as well as the efficacy of all tested ligands (Table 5 and Fig. 8C and D). The increased basal activity was followed by a corresponding increase in the efficacy of rosiglitazone confirming the hypothesis that this mutation might cause a proper arrangements of H12.

The same amino acid substitution of PPARγ did not affect the potency of all the tested ligands. Therefore the methionine, when substituted with the less obstructing residue alanine, could determine less ligand efficacy while retaining similar potency of all tested ligands. This suggests that this amino acid residue allows a binding mode of agonists leading to suboptimal conformation for recruitment of co-regulators required for full receptor activation.

4. Conclusions

By using an integrated approach carried out on a series of chiral PPAR agonists 2D, 3D-QSAR, and docking, provided a tool to gain valid information on the chemical and structural characteristic most likely related to an increased PPARα and/or PPARγ activity. Site-directed mutagenesis study carried out on the insights from the modelling identifies the elements that are important for PPARα/γ selectivity, suggesting that agonists might elicit (or indeed hamper) a significant receptor activation interfering with certain residues, located in a more flexible region of the ligand binding domain, according to their enhanced (or reduced) lipophilicity and steric hindrance.

The mutagenesis also prompted us to a more introspective evaluation of this features, and this is an ongoing project we are carrying out through molecular dynamics simulations on both the wild type and the *in silico* mutants of PPARs. As a consequence and in perspective this tool will be then useful in the design of new ligands for these biological targets that may provide potential leads for the treatment of diabetes, MS or other severe CVDs.

Acknowledgements

This work was accomplished thanks to the financial support of the Ministero dell'Istruzione, dell'Università e della Ricerca (MIUR 2005033023 and PRIN 2009K7R7NA), the Cariplo Foundation 2009.2727 and the Università degli Studi di Bari "Aldo Moro" ("IDEA Giovani Ricercatori" GRBA1107J2).

References

[1] Causes of Death, World Health Organization, Geneva, 2008. http://www.who.int/healthinfo/global_burden_disease/cod_2008_sources_methods.pdf.
[2] R.H. Eckel, S.M. Grundy, P.Z. Zimmet, The metabolic syndrome, The Lancet 365 (9468) (2005) 1415–1428.
[3] P. Zimmet, K.G.M.M. Alberti, J. Shaw, Global and societal implications of the diabetes epidemic, Nature 414 (2001) 782–787.
[4] C.S. Flordellis, I. Ilias, A.G. Papavassiliou, New therapeutic options for the metabolic syndrome: what's next? Trends Endocrinol. Metab. 16 (6) (2005) 254–260.
[5] S.M. Grundy, H.B. Brewer Jr., J.I. Cleeman, S.C. Smith Jr., C. Lenfant, Definition of metabolic syndrome: report of the National Heart, Lung, and Blood Institute/American Heart Association conference on scientific issues related to definition, Circulation 109 (3) (2004) 433–438.
[6] P.T. James, N. Rigby, R. Leach, The obesity epidemic, metabolic syndrome and future prevention strategies, Eur. J. Cardiovasc. Prev. Rehabil. 11 (1) (2004) 3–8.
[7] E.N. Liberopoulos, D.P. Mikhailidis, M.S. Elisaf, Diagnosis and management of the metabolic syndrome in obesity, Obes. Rev. 6 (4) (2005) 283–296.
[8] S. Nammi, K. Saisudha, M. Chinnala Krishna, M. Boini Krishna, Obesity: an overview on its current perspectives and treatment options, Nutr. J. 3 (3) (2004) 1–8.
[9] M.H. Moneva, S. Dagogo-Jack, Multiple drug targets in the management of type 2 diabetes, Curr. Drug Targets 3 (3) (2002) 203–221.
[10] B. Hulin, New hypoglycaemic agents, Prog. Med. Chem. 31 (1994) 1–58.
[11] B. Pourcet, J.C. Fruchart, B. Staels, C. Glineur, Selective PPAR modulators, dual and pan PPAR agonists: multimodal drugs for the treatment of type 2 diabetes and atherosclerosis, Expert Opin. Emerging Drugs 11 (3) (2006) 379–401.
[12] I. Issemann, S. Green, Activation of a member of the steroid hormone receptor superfamily by peroxisome proliferators, Nature 347 (6294) (1990) 645–650.
[13] T.M. Willson, P.J. Brown, D.D. Sternbach, D.R. Henke, The PPARs: from orphan receptors to drug discovery, J. Med. Chem. 43 (4) (2000) 527–550.
[14] R.W. Nesto, D. Bell, R.O. Bonow, V. Fonseca, S.M. Grundy, E.S. Horton, M. Le Winter, D. Porte, C.F. Semenkovich, S. Smith, L.H. Young, R. Kahn, Thiazolidinedione use, fluid retention, and congestive heart failure: a consensus statement from the American Heart Association and American Diabetes Association, Diabetes Care 27 (2004) 256–263.
[15] M. Bodmer, C. Meier, M.E. Kraenzlin, C.R. Meier, Risk of fractures with glitazones: a critical review of the evidence to date, Drug Saf. 32 (2009) 539–547.
[16] A. Pinelli, C. Godio, A. Laghezza, N. Mitro, G. Fracchiolla, V. Tortorella, A. Lavecchia, E. Novellino, J.C. Fruchart, B. Staels, M. Crestani, F. Loiodice, Synthesis, biological evaluation, and molecular modeling investigation of new chiral fibrates with PPARalpha and PPARgamma agonist activity, J. Med. Chem. 48 (2005) 5509–5519.
[17] G. Fracchiolla, A. Laghezza, L. Piemontese, G. Carbonara, A. Lavecchia, P. Tortorella, M. Crestani, E. Novellino, F. Loiodice, Synthesis, biological evaluation, and molecular modeling investigation of chiral phenoxyacetic acid analogues with PPARalpha and PPARgamma agonist activity, ChemMedChem 2 (2007) 641–654.
[18] G. Fracchiolla, A. Lavecchia, A. Laghezza, L. Piemontese, R. Trisolini, G. Carbonara, P. Tortorella, E. Novellino, F. Loiodice, Synthesis, biological evaluation, and molecular modeling investigation of chiral 2-(4-chloro-phenoxy)-3-phenyl-propanoic acid derivatives with PPARalpha and PPARgamma agonist activity, Bioorg. Med. Chem. 16 (2008) 9498–9510.
[19] G. Fracchiolla, A. Laghezza, L. Piemontese, P. Tortorella, F. Mazza, R. Montanari, G. Pochetti, A. Lavecchia, E. Novellino, S. Pierno, D. Conte Camerino, F. Loiodice, New 2-aryloxy-3-phenyl-propanoic acids as peroxisome proliferator-activated receptors alpha/gamma dual agonists with improved potency and reduced adverse effects on skeletal muscle function, J. Med. Chem. 52 (2009) 6382–6393.
[20] G. Fracchiolla, A. Laghezza, L. Piemontese, M. Parente, A. Lavecchia, G. Pochetti, R. Montanari, C. Di Giovanni, G. Carbonara, P. Tortorella, E. Novellino, F. Loiodice, Synthesis, biological evaluation and molecular investigation of fluorinated peroxisome proliferator-activated receptors α/γ dual agonists, Bioorg. Med. Chem. 20 (6) (2012) 2141–2151.
[21] L. Porcelli, F. Gilardi, A. Laghezza, L. Piemontese, N. Mitro, A. Azzariti, F. Altieri, L. Cervoni, G. Fracchiolla, M. Giudici, U. Guerrini, A. Lavecchia, R. Montanari, C. Di Giovanni, A. Paradiso, G. Pochetti, G.M. Simone, P. Tortorella, M. Crestani, F. Loiodice, Synthesis, characterization and biological evaluation of ureidofibrate-like derivatives endowed with peroxisome proliferator-activated receptor activity, J. Med. Chem. 55 (1) (2012) 37–54.
[22] R. Montanari, F. Saccoccia, E. Scotti, M. Crestani, C. Godio, F. Gilardi, F. Loiodice, G. Fracchiolla, A. Laghezza, P. Tortorella, A. Lavecchia, E. Novellino, F. Mazza, M. Aschi, G. Pochetti, Crystal structure of the peroxisome proliferator-activated receptor gamma (PPARgamma) ligand binding domain complexed with a novel partial agonist: a new region of the hydrophobic pocket could be exploited for drug design, J. Med. Chem. 51 (2008) 7768–7776.
[23] G. Pochetti, C. Godio, N. Mitro, D. Caruso, A. Galmozzi, S. Scurati, F. Loiodice, G. Fracchiolla, P. Tortorella, A. Laghezza, A. Lavecchia, E. Novellino, F. Mazza, M. Crestani, Insights into the mechanism of partial agonism: crystal structures of the peroxisome proliferator-activated receptor gamma ligand-binding domain in the complex with two enantiomeric ligands, J. Biol. Chem. 282 (2007) 17314–17324.
[24] G. Pochetti, N. Mitro, A. Lavecchia, F. Gilardi, N. Besker, E. Scotti, M. Aschi, N. Re, G. Fracchiolla, A. Laghezza, P. Tortorella, R. Montanari, E. Novellino, F. Mazza, M. Crestani, F. Loiodice, Structural insight into peroxisome proliferator-activated receptor gamma binding of two ureidofibrate-like enantiomers by molecular dynamics, cofactor interaction analysis, and site-directed mutagenesis, J. Med. Chem. 53 (11) (2010) 4354–4366.

[25] A. Carrieri, A. Piergentili, F.D. Bello, M. Giannella, M. Pigini, A. Leonardi, F. Fanelli, W. Quaglia, Structure-activity relationships in 1,4-benzodioxan-related compounds. 10. Novel α1-adrenoreceptor antagonists related to openphendioxan: synthesis, biological evaluation, and α1d computational study, Bioorg. Med. Chem. 18 (2010) 7065–7077.
[26] A. Carrieri, V.I. Pérez-Nueno, A. Fano, C. Pistone, D.W. Ritchie, J. Teixidó, Biological profiling of anti-HIV agents and insight into CCR5 antagonist binding using in silico techniques, ChemMedChem 4 (2009) 1153–1163.
[27] A. Carrieri, M. Muraglia, F. Corbo, C. Pacifico, 2D- and 3D-QSAR of tocainide and mexiletine analogues acting as Na(v)1.4 channel blockers, Eur. J. Med. Chem. 44 (2009) 1477–1485.
[28] MacroModel, Version 9.9, Schrödinger, LLC, New York, NY, 2012.
[29] QikProp, Version 3.5, Schrödinger, LLC, New York, NY, 2012.
[30] W. Wang, P. Devasthale, D. Farrelly, L. Gu, T. Harrity, M. Cap, C. Chu, L. Kunselman, N. Morgan, R. Ponticiello, R. Zebo, L. Zhang, K. Locke, J. Lippy, K. O'Malley, V. Hosagrahara, L. Zhang, P. Kadiyala, C. Chang, J. Muckelbauer, A.M. Doweyko, R. Zahler, D. Ryono, N. Hariharan, P.T. Cheng, Discovery of azetidinone acids as conformationally-constrained dual PPARalpha/gamma agonists, Bioorg. Med. Chem. Lett. 18 (2008) 1939–1944.
[31] Maestro, Version 9.3, Schrödinger, LLC, New York, NY, 2012.
[32] G.M. Morris, R. Huey, W. Lindstrom, M.F. Sanner, R.K. Belew, D.S. Goodsell, A.J. Olson, AutoDock4 and AutoDockTools4: automated docking with selective receptor flexibility, J. Comput. Chem. 16 (2009) 2785–2791.
[33] A. Sali, T.L. Blundell, Comparative protein modelling by satisfaction of spatial restraints, J. Mol. Biol. 234 (1993) 779–815.
[34] GRID Version 22c, Molecular Discovery Ltd., 4 Chandos Street, London W1A3BQ, 2012. http://www.moldiscovery.com.
[35] P.J. Goodford, A computational procedure for determining energetically favorable binding sites on biologically important macromolecules, J. Med. Chem. 28 (1985) 849–857.
[36] M. Pastor, G. Cruciani, I. Mclay, S. Pickett, S. Clementi, GRid-INdependent descriptors (GRIND): a novel class of alignment-independent three-dimensional molecular descriptors, J. Med. Chem. 43 (2000) 3233–3243.
[37] F. Fontaine, M. Pastor, I. Zamora, F. Sanz, Anchor-GRIND: filling the gap between standard 3D QSAR and the GRid-INdependent descriptors, J. Med. Chem. 48 (7) (2005) 2687–2694.
[38] G.M. Morris, D.S. Goodsell, R.S. Halliday, R. Huey, W.E. Hart, R.K. Belew, A.J. Olson, Automated docking using a lamarckian genetic algorithm and empirical binding free energy function, J. Comput. Chem. 19 (1998) 1639–1662.
[39] P. Ferrara, H. Gohlke, D.J. Price, G. Klebe, C.L. Brooks 3rd, Assessing scoring functions for protein-ligand interactions, J. Med. Chem. 47 (2004) 3032–3047.